

Raman spectroscopy detects deterioration in biomechanical properties of bone in a glucocorticoid-treated mouse model of rheumatoid arthritis

Jason R. Maher
Masahiko Takahata
Hani A. Awad
Andrew J. Berger

Raman spectroscopy detects deterioration in biomechanical properties of bone in a glucocorticoid-treated mouse model of rheumatoid arthritis

Jason R. Maher,^{a,*} Masahiko Takahata,^{b,*} Hani A. Awad,^{b,c} and Andrew J. Berger^{a,c}

^aUniversity of Rochester, The Institute of Optics, Rochester, New York 14627

^bUniversity of Rochester, The Center for Musculoskeletal Research, Rochester, New York 14642

^cUniversity of Rochester, Department of Biomedical Engineering, Rochester, New York 14627

Abstract. Although glucocorticoids are frequently prescribed for the symptomatic management of inflammatory disorders such as rheumatoid arthritis, extended glucocorticoid exposure is the leading cause of physician-induced osteoporosis and leaves patients at a high risk of fracture. To study the biochemical effects of glucocorticoid exposure and how they might affect biomechanical properties of the bone, Raman spectra were acquired from *ex vivo* tibiae of glucocorticoid- and placebo-treated wild-type mice and a transgenic mouse model of rheumatoid arthritis. Statistically significant spectral differences were observed due to both treatment regimen and mouse genotype. These differences are attributed to changes in the overall bone mineral composition, as well as the degree of phosphate mineralization in tibial cortical bone. In addition, partial least squares regression was used to generate a Raman-based prediction of each tibia's biomechanical strength as quantified by a torsion test. The Raman-based predictions were as accurate as those produced by microcomputed tomography derived parameters, and more accurate than the clinically-used parameter of bone mineral density. These results suggest that Raman spectroscopy could be a valuable tool for monitoring bone biochemistry in studies of bone diseases such as osteoporosis, including tests of drugs being developed to combat these diseases. © 2011 Society of Photo-Optical Instrumentation Engineers (SPIE). [DOI: 10.1117/1.3613933]

Keywords: Raman spectroscopy; bone; osteoporosis; rheumatoid arthritis; biomechanics; partial least squares.

Paper 11149PR received Mar. 25, 2011; revised manuscript received Jun. 20, 2011; accepted for publication Jun. 29, 2011; published online Aug. 16, 2011.

1 Introduction

Arthritis and other rheumatic conditions represent a public health burden that is both significant and growing. In 2008, it was estimated that more than 21% of U.S. adults (46.4 million persons) were diagnosed with some type of arthritis, with rheumatoid arthritis affecting 1.3 million patients.¹

Glucocorticoids are among the most extensively used anti-inflammatory agents in the management of the painful symptoms of rheumatoid arthritis. However, since the glucocorticoid (GC) receptor is expressed in almost every cell in the body, glucocorticoids have many effects, including potentially harmful ones on bone metabolism. These adverse effects include inhibition of bone formation and an enhancement of bone resorption, often leading to osteoporosis, and ultimately an increased risk of fracture. Currently, extended exposure to glucocorticoids is the leading cause of physician-induced osteoporosis, leaving patients susceptible to fractures at reported rates of 30% to 50%.² It has also been shown that GC excess in mice affects bone metabolism in a similar fashion, leading to significant osteoporosis that mimics clinical symptoms in human patients.²⁻⁴

To reverse GC-induced osteoporosis, several classes of drugs have been developed, including antiresorptive drugs of the bisphosphonate family⁵⁻⁷ and anti-tumor necrosis factor (TNF) drugs.⁸ Clinical trials of these drugs typically report increases in bone mineral density (BMD), as measured by dual energy x-ray absorptiometry (DXA) or computed tomography, as the primary outcome of drug efficacy. However, this increase in BMD is not predictive of fracture risk in the nearly 10% of treated patients that experience a fracture.^{9,10} Therefore, new diagnostic and monitoring technologies for detection of bone changes that better correlate with fracture risk could potentially be more definitive than BMD in establishing the efficacy of new generations of these drugs.

Vibrational spectroscopic techniques, including Raman spectroscopy, have been used extensively to study bone and other mineralized tissue.^{11,12} In particular, the bone diseases postmenopausal osteoporosis,¹³ osteogenesis imperfecta,¹⁴ and early-onset osteoarthritis¹⁵ all induce perturbations to cortical bone that can be detected by Raman spectroscopy. In this communication, we report the results of the first Raman spectroscopy study of cortical bone in a transgenic mouse model of rheumatoid arthritis that constitutively overexpresses the inflammatory molecule human tumor necrosis factor-alpha (hTNF- α), which was developed by Keffer et al.¹⁶ Because of its chronic progressive nature, 100% incidence, and simple etiology, the hTNF- α

*Contributed equally to this article.

Address all correspondence to: Andrew J. Berger, University of Rochester, The Institute of Optics, 405 Goergen Hall, Rochester, NY 14627; Tel: 585-273-4724; Fax: 585-244-4936; E-mail: ajberger@optics.rochester.edu.

transgenic (hTNF-Tg) mouse is an excellent model to investigate the pathogenesis and treatment of rheumatoid arthritis and side effects such as GC-induced osteoporosis.

2 Materials and Methods

2.1 Specimens

Five month old hTNF-Tg mice (3647 line originally obtained from Dr. G. Kollias and maintained as heterozygotes in a CBA \times C57Bl6 background)¹⁷ and wild-type (WT) littermates (C57Bl6 strain) were randomized into placebo (PL) or GC treatment groups. Placebo pellets were implanted subcutaneously in group 1 (WT PL, $N = 4$) and group 3 (hTNF-Tg PL, $N = 3$) mice, while group 2 (WT GC, $N = 4$) and group 4 (hTNF-Tg GC, $N = 4$) were implanted with a slow-release pellet (5 mg/kg/day) of the glucocorticoid Prednisolone (Innovative Research of America, Sarasota, Florida) as described by Lane et al.¹⁸ Following a 6-week treatment period, the mice were sacrificed and the left tibiae were excised and evaluated by microcomputed tomography (microCT), Raman spectroscopy, and biomechanical testing. The tibiae were stored in phosphate buffered saline between measurements. A sample size of $N = 4$ mice/group was chosen for this preliminary study; however, one mouse from group 3 was lost due to premature death.

2.2 Microcomputed Tomography

MicroCT measurements were performed on a Scanco VivaCT 40 (Scanco Medical AG, Bassersdorf, Switzerland) with a 10.5- μm isotropic resolution. In addition to the whole BMD, 4 cortical parameters related to torsional biomechanics (cortical BMD, cortical thickness, polar moment of inertia, and bone area) were measured. The whole BMD was measured in the proximal half of the tibia. The cortical BMD and thickness were measured over 100 axial slices from the center of the diaphysis. Each parameter was calculated from three-dimensional reconstructions of the microCT scans generated by the provided complete image solution software (Scanco Medical, Bassersdorf, Switzerland).

2.3 Raman Spectroscopy

Raman spectra were acquired from the medial side of the proximal, distal, and mid-diaphysis regions of the excised tibiae with an exposure time of 300 s per region. These measurements were performed on a locally constructed Raman spectroscopy system that utilized an 830-nm semiconductor laser (Model PI-ECL-830-500-FS, Process Instruments Inc., Salt Lake City, Utah) for excitation. The laser light was filtered with a bandpass filter (Chroma Technology Corp., Bellows Falls, Vermont) and focused to a 1.5-mm ($1/e^2$ full-width) spot on the surface of the bone. The total power delivered to the specimen was approximately 80 mW and the illumination numerical aperture was 0.05.

In order to collect the Raman scattered light, the illuminated surface region was imaged onto the face of an optical fiber bundle. The fiber bundle consisted of 61 multimode optical fibers with 100/120- μm core/cladding diameters in a circular array at the collection end mapped to a linear array at the delivery end. Due to the system magnification, the diameter of the fiber bundle image was 1.5 mm and each fiber viewed a 285- μm diameter spot at the surface of the bone. Following

collection, the scattered light was delivered to a spectrograph (HolospecTM VPT System, Kaiser Optical Systems Inc., Ann Arbor, Michigan) where it was dispersed onto a 1024 \times 256 array back-illuminated deep-depletion charge-coupled device (CCD) camera (Model DU 420-BR-DD, Andor Technology, Belfast, Northern Ireland), achieving a spectral resolution of approximately 5 cm^{-1} . A dichroic beam splitter (Chroma Technology Corp., Bellows Falls, Vermont) and a holographic notch filter (Kaiser Optical Systems Inc., Ann Arbor, Michigan) were used to reject the elastically scattered light and pass only the Stokes-shifted light to the spectrograph. During acquisitions, the CCD was thermoelectrically cooled to -60°C to suppress electronic noise due to thermal fluctuations. Finally, because of the limited height of the CCD array, only spectra from the 40 central fibers of the fiber bundle were imaged onto the CCD.

2.4 Spectroscopic Data Processing

Full CCD spectral images were imported into MATLAB[®] (version 7.8, The MathWorksTM, Natick, Massachusetts) for analysis. Spectral processing included cosmic ray removal, readout and dark-current subtraction, and correction for the frequency-dependent response of the system. A nonlinear spatial transformation was applied to each image in order to correct for optical aberrations in the spectrograph system in a manner similar to that described by Esmonde-White et al.¹⁹ The spectrum of Raman scattered light collected by each fiber was extracted from the full image by fitting to the separately measured spectral response of each fiber.²⁰

All spectra were truncated to the 825 to 1750 cm^{-1} region, which includes many relevant mineral and organic matrix bands.¹² The lower spectral cutoff was chosen due to the presence of a strong uncorrelated fluorescence contribution below 825 cm^{-1} . Following spectral truncation, the background fluorescence lineshapes were modeled and removed through the use of an iterative polynomial fitting routine.²¹ Next, the spectra were normalized to the area under the amide I peak in the 1625 to 1725 cm^{-1} region and smoothed with a Savitzky-Golay filter²² over a 3 pixel (approximately 5 cm^{-1}) window, chosen to match the resolution of the spectrograph. The spectra from each bone [≤ 120 total; ≤ 40 spectra per region (1 per fiber) \times 3 regions] were averaged, yielding a single Raman spectrum per tibia. Spectra with a large amount of high frequency noise relative to Raman signal, due to either a large fluorescence-to-Raman ratio or a small amount of absolute Raman signal, were discarded before averaging. The amount of high frequency noise in a spectrum was quantified by calculating $Z_i = \langle |S''_{v,i}| \rangle$ where $S''_{v,i}$ is the second derivative of the i 'th spectrum with respect to wavenumber shift and the angle brackets denote an average over wavenumber shift. The median, \bar{Z} , and median absolute deviation, δ , were used to identify and remove outliers ($Z_i > \bar{Z} + 2\delta$). Finally, the wavenumber axis was calibrated with N-acetyl-para-aminophenol, better known by the brand name TYLENOL[®] (McNEIL-PPC Inc., Fort Washington, Pennsylvania), to correct for spectral instabilities in the excitation source.

2.5 Biomechanical Testing

Following microCT and Raman measurements, the tibiae were tested in torsion, as previously described.²³ Briefly, the ends of the tibiae were cemented into square 6.35-mm² aluminum tube

holders using polymethylmethacrylate bone cement (DePuy Orthopaedics, Inc., Warsaw, Indiana) in order to maintain a 4-mm gauge length over the proximal 1/3 of the tibial diaphysis. Following this procedure, the specimens were bathed in phosphate buffered saline at room temperature for at least 2 h in order to allow for rehydration of the tissue.²⁴ Specimens were then mounted on an EnduraTec TestBench™ system (200 N-mm torque cell; Bose Corporation, Minnetonka, Minnesota) and loaded monotonically in torsion at a rate of 1°/s until failure.²⁵ The torque data were plotted against the rotational deformation (normalized by the gauge length and expressed as rad/mm) to determine the ultimate torque (maximum applied torque prior to fracture). The root-mean-squared error in the ultimate torque measurement was 0.2 N-mm.

It should be noted that torsional testing was chosen for this study since it represents a mode of loading that commonly leads to long bone fractures in humans. However, qualitatively similar results would be expected from bending tests since similarities in the results of these tests have been reported during skeletal growth²⁵ and in a model of skeletal fragility.²⁶

2.6 Data Analysis

The effects of treatment regimen (PL versus GC) and mouse genotype (WT versus hTNF-Tg) on ultimate torque, BMD, cortical thickness, and Raman band area ratios were examined using a two-way analysis of variance (ANOVA) model. All statistical analyses were performed in MATLAB® and significance was set at $p \leq 0.05$.

Following these tests on the ensemble-averaged properties of each group, correlations were sought at the single-bone level between ultimate torque and various microCT- and Raman-derived parameters. Because of the small sample size, a leave-one-out cross-validation (LOOCV) approach was used to generate

microCT- and Raman-based predictions of ultimate torque for each tibia, based upon calibration using the other 14. First, a univariate prediction model was built using BMD as a predictor variable. A more complex model was built using multiple microCT-derived parameters (cortical BMD, cortical thickness, polar moment of inertia, and bone area), via partial least squares regression (PLSR).²⁷ PLSR was also used to generate predictions based upon spectral data, either from selected Raman peaks (discussed below) or from the entire Raman spectrum.

The rank of the PLSR model used for each prediction was selected based upon the method described by Haaland and Thomas²⁷ applied to an inner cross-validation performed upon each calibration set. In addition, in order to further prevent overfitting the calibration data, the number of samples in the calibration set was required to be at least 3 times larger than the rank of the selected model.²⁸ Following prediction, the accuracy of each technique was assessed by calculating the root-mean-squared error of cross-validation (RMSECV).

3 Results

The average Raman spectra acquired from each of the 15 mice are overlaid in Fig. 1. Major Raman bands associated with mineral (PO_4^{3-} and CO_3^{2-}) and protein matrix (amide III, CH_2 , and amide I) content are labeled. Band area ratios frequently studied in vibrational spectroscopic analysis of diseased cortical bone include the mineral-to-matrix ratio (MTMR; $\text{PO}_4^{3-}/\text{CH}_2$ or $\text{PO}_4^{3-}/\text{amide I}$), which describes the degree of phosphate mineralization, and the phosphate-to-carbonate ratio (PTCR; $\text{PO}_4^{3-}/\text{CO}_3^{2-}$), which describes the amount of carbonate substitution in the apatite crystal lattice.^{13,15} Since all spectra have been normalized to the area under the amide I peak, variation in the MTMR is represented by the variation in the PO_4^{3-} peak near 960 cm^{-1} . The spectral insets in Fig. 1 highlight this variation,

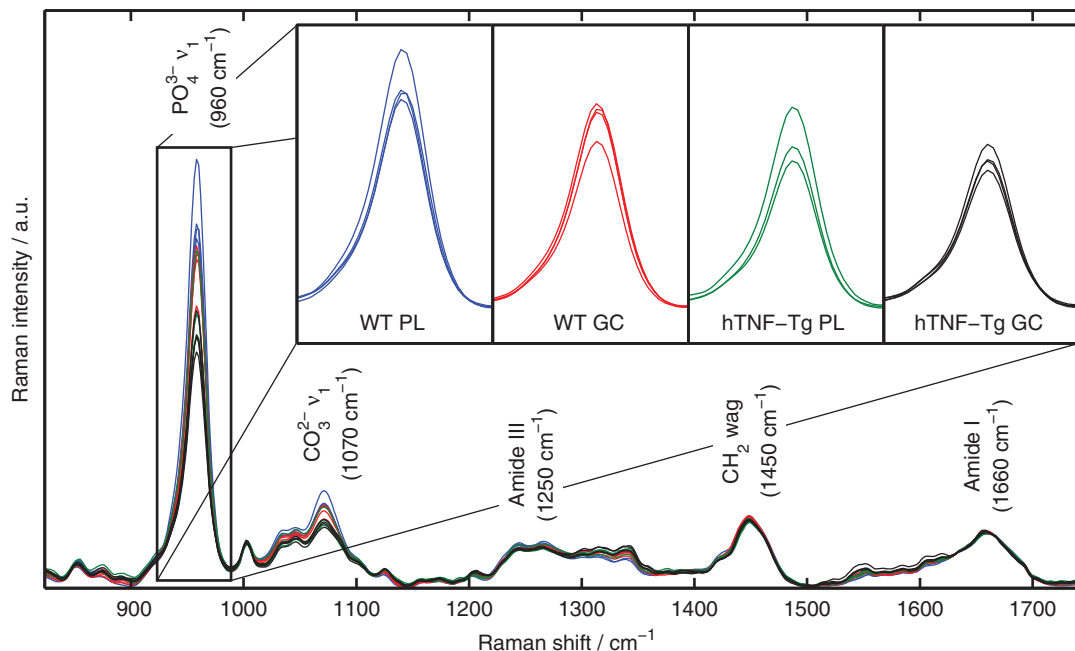


Fig. 1 Mean Raman spectra from each of the tibiae. The major Raman bands are labeled along with their peak positions (in parentheses) in relative wavenumber shift. The spectral insets highlight the variation in the mineral-to-matrix ratio (specifically, the band area ratio of PO_4^{3-} to amide I) between the four groups of mice. (Color online only.)

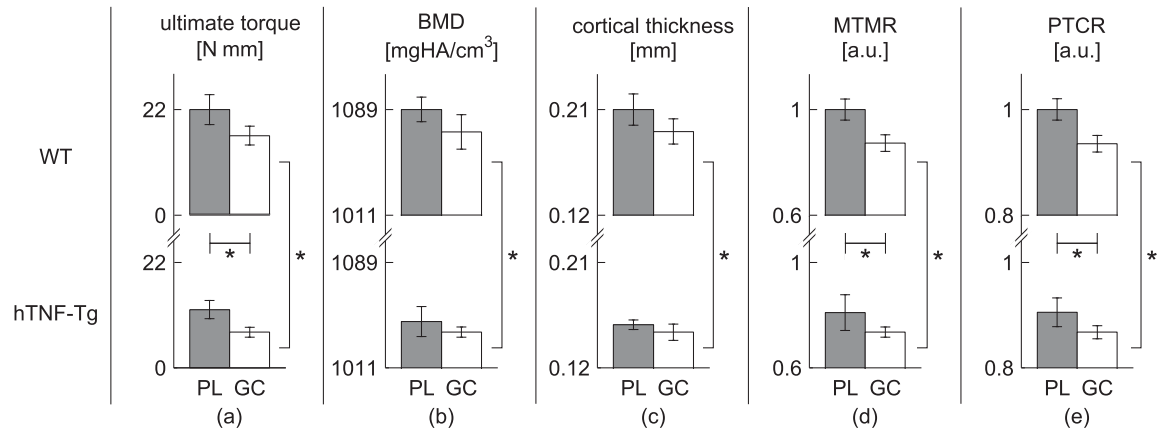


Fig. 2 Bar plots of the mean (a) ultimate torque, (b) BMD, (c) cortical thickness, (d) MTMR, and (e) PTCR of each group. The error bars are plotted as the standard error of the mean. The gray bars represent PL-treated groups and the white bars represent GC-treated groups. * $p \leq 0.05$ as determined by two-way ANOVA.

showing a decrease in the MTMR dependent upon treatment regimen and mouse genotype.

The ensemble-averaged ultimate torque, BMD, cortical thickness, MTMR, and PTCR for each group of mice are presented in Fig. 2. Trends are readily visible for all five parameters: they decrease with GC treatment and also in transgenic mice. For ultimate torque and the Raman-based parameters, both of these trends were significant (as determined by two-way ANOVA); for the microCT parameters, only the mouse genotype was found to be significant. The magnitudes of the standardized ultimate torque effect sizes (along with 95% confidence intervals) were 1.20 [0.07,2.34], 2.25 [1.11,3.39], and 0.09 [0,1.22] for the treatment, genotype, and interaction effects, respectively. Only the main effects of treatment regimen and mouse genotype were included in the final ANOVA models since the interaction effects were not statistically significant.

Figure 3 provides scatter plots of ultimate torque as predicted by regression against BMD alone (a), multiple microCT parameters (b), and the full Raman spectrum (c). All of the plots show significant correlation between the measured and predicted values of ultimate torque, with the BMD plot being noticeably noisier. The accuracy of each prediction model is quantified in Table 1.

In order to isolate the Raman spectral features most associated with compromised bone strength, a Raman peak-based

prediction algorithm was also sought. The Raman spectral features that were most predictive of ultimate torque were identified by analyzing the PLSR coefficients as described by Beier et al.²⁹ Briefly, the Hadamard, or entrywise, product of the mean-centered spectrum of the tibia with the largest ultimate torque, $S_{\bar{v}}$, and the regression coefficients generated by PLSR, $b_{\bar{v}}$, was calculated. By definition, this vector ($b_{\bar{v}} \circ S_{\bar{v}}$) assigns large absolute values to spectral regions with high predictive power. Analysis of the $b_{\bar{v}} \circ S_{\bar{v}}$ spectrum revealed that the PO_4^{3-} , CO_3^{2-} , and CH_2 peaks were strongly leveraged in predicting ultimate torque. A separate peak-based prediction model was built using the areas under the PO_4^{3-} , CO_3^{2-} , and CH_2 peaks, as well as the first moment of the PO_4^{3-} peak, which is related to the peak's spectral location. Using a LOOCV approach, these four Raman parameters were used to predict the ultimate torque of each bone. The prediction accuracy of this model is included in Table 1.

4 Discussion

The trend in the ensemble-averaged measurements of the microCT-derived BMD and Raman spectroscopy derived MTMR closely matches the biomechanical ultimate torque measurements as seen in Fig. 2. The BMD and MTMR measurements suggest that both the total mineral content and phosphate

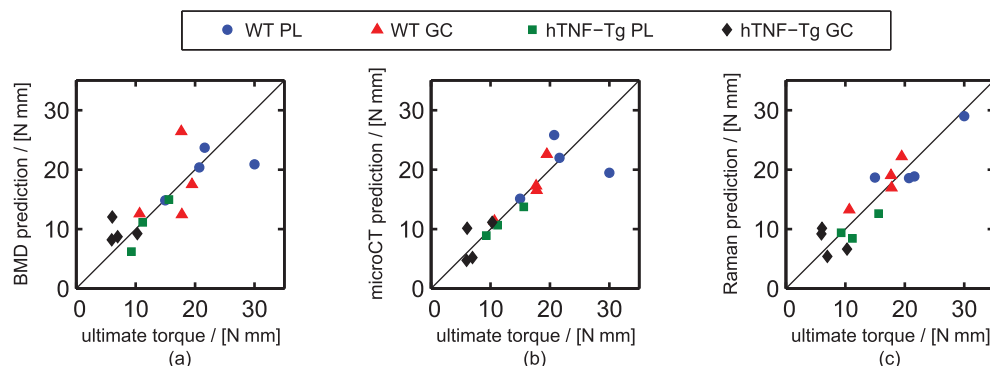


Fig. 3 Scatter plots of the ultimate torque prediction for each tibia versus its measured value for the (a) BMD, (b) microCT PLSR, and (c) Raman PLSR prediction models. The RMSECV of each prediction model is presented in Table 1. (Color online only.)

Table 1 Accuracy of ultimate torque prediction.

Technique	Predictor/s	RMSECV (N·mm)
microCT (or DXA)	BMD	4.1
microCT	PLSR of 4 parameters	3.4
Raman	MTMR	4.5
Raman	PTCR	4.6
Raman	PLSR of 4 parameters	2.7
Raman	PLSR of full spectrum	2.6

mineral content relative to the protein matrix are reduced in the bones of GC-treated and hTNF-Tg mice. Hypomineralization is expected in each of these cases since both GC-treatment and arthritic inflammation decrease bone formation and increase bone resorption.³⁰ The concomitant decrease in the PTCR implies that the degree of carbonate substitution in the apatite crystal lattice is larger in the bones of GC-treated and hTNF-Tg mice compared to the wild-type controls. Others have reported a similar decrease in the PTCR in women who had experienced an osteoporotic fracture.¹³

The fact that statistically significant interaction effects were not observed in this study may be due to the relatively small sample size (15 total specimens). Potentially relevant ultimate torque effect sizes are those greater than about 2.6 N·mm (the prediction accuracy of the full-spectrum Raman PLSR model), which corresponds to a standardized effect size of about 0.6. Further study of the interaction between glucocorticoid treatment and mouse genotype is warranted since this effect size, as well as an effect size of zero, is included in the 95% confidence interval for the magnitude of the ultimate torque interaction effect [0,1.22].

The regression models for prediction presented in Fig. 3 and Table 1 suggest that Raman signatures from bone, if obtained transcutaneously, may be capable of screening for fracture risk more reliably than the conventional measurement of BMD via DXA or computed tomography. DXA is the current standard for diagnosing osteoporosis since it is the most extensively validated technology for clinical prediction of fracture risk.³¹ Computed tomography can also be used to measure BMD and provides additional quantitative information about bone structure. However, computed tomography requires a higher radiation dose and remains more expensive and less accessible than DXA. The scatter plots in Fig. 3, along with Table 1, provide estimates of the fracture risk prediction accuracy of DXA [Fig. 3(a)], computed tomography [Fig. 3(b)], and Raman spectroscopy [Fig. 3(c)]. Among these technologies, Raman spectroscopy produced the smallest prediction error. Raman spectroscopy could also provide a potential cost and space benefit over clinical DXA and computed tomography scanners, and it is arguably safer as it does not require the use of ionizing radiation. While transcutaneous acquisition of bone Raman signatures will inevitably reduce the signal strength, the ability to acquire such spectra in mice,^{32,33} rats,³⁴ chickens,³⁴ canines,³⁵ and humans³⁶ has recently been demonstrated.

Previous Raman spectroscopy studies of osteoporotic bone have primarily focused on changes to individual spectral features associated with specific biochemical properties of the bone.¹¹ Recent studies have also revealed correlations between various Raman spectral features and a number of parameters related to the bone's biomechanical strength.³⁷⁻³⁹ Specifically, correlations between the ultimate stress (maximum applied stress prior to fracture) and the Raman-derived MTMR and crystallinity (which is related to the inverse of the $\text{PO}_4^{3-} \nu_1$ peak width) have been observed in the femurs of rats and mice. The present results emphasize that full-spectrum regression methods such as PLSR can often provide stronger correlations with biomechanical properties. For comparison to PLSR, simple univariate models for predicting ultimate torque were built based upon single Raman band area ratios (MTMR and PTCR). While these ratios have shown potential for diagnosing osteoporosis,¹¹ the MTMR and PTCR both proved to be poor univariate predictors of ultimate torque (RMSECV = 4.5 and 4.6 N·mm, respectively), compared to the more advanced PLSR modeling (Table 1). This underscores the importance of using the full plethora of spectral data, rather than a single spectral feature, for predicting the biomechanical properties of a bone.

This study is the first to evaluate bone changes using a variety of minimally invasive imaging and spectroscopic techniques and to establish predictive correlations with the biomechanical properties of cortical bone in a mouse model of rheumatoid arthritis. The data presented here examined mice at only a single GC-exposure time point (6 weeks). Interesting future directions include examining mice at earlier time points to evaluate whether Raman spectroscopy can predict early, subtle chemical changes to the bone before later changes in BMD and deterioration of biomechanical properties are manifest. Toward clinical translation of this diagnostic technology, longitudinal *in vivo* studies in mice utilizing transcutaneous detection will also be pursued.

5 Conclusion

Raman spectroscopy has been used to study the chemical perturbations to cortical bone associated with both glucocorticoid-induced osteoporosis and rheumatoid arthritis. Each disease was associated with statistically significant changes in the degree of phosphate mineralization and overall mineral composition in the tibial cortical bone of mice. Raman spectroscopy and micro-computed tomography were also separately used to predict tibial fracture risk as quantified by a biomechanical measurement of ultimate torque (maximum applied torque prior to fracture). Predictions based upon the measured Raman spectrum were as accurate as those produced by microcomputed tomography derived parameters, and more accurate than the clinically-used parameter of bone mineral density.

Acknowledgments

This work was supported in part by a University of Rochester Provost's Multidisciplinary Award and NIH Grant No. 1R21AR061285-01. We would like to thank Dr. Edward Schwarz for valuable advice and for providing the breeder mice for the hTNF-Tg mouse colony used in this study, Dr. Subhash Juneja for his help with maintaining and genotyping the hTNF-Tg mouse colony, and Mr. Michael Thullen for his excellent technical assistance with the microcomputed tomography analysis.

References

- C. G. Helmick, D. T. Felson, R. C. Lawrence, S. Gabriel, R. Hirsch, C. K. Kwoh, M. H. Lian, H. M. Kremers, M. D. Mayes, P. A. Merkel, S. R. Pillemer, J. D. Reveille, and J. H. Stone, "Estimates of the prevalence of arthritis and other rheumatic conditions in the United States. Part I," *Arthritis Rheum.* **58**, 15–25 (2008).
- S. C. Manolagas and R. S. Weinstein, "New developments in the pathogenesis and treatment of steroid-induced osteoporosis," *J. Bone Miner. Res.* **14**, 1161–1066 (1999).
- W. Yao, Z. Cheng, A. Pham, C. Busse, E. A. Zimmermann, R. O. Ritchie, and N. E. Lane, "Glucocorticoid-induced bone loss in mice can be reversed by the actions of parathyroid hormone and risedronate on different pathways for bone formation and mineralization," *Arthritis Rheum.* **58**, 34853497 (2008).
- R. S. Weinstein, R. L. Jilka, A. M. Parfitt, and S. C. Manolagas, "Inhibition of osteoblastogenesis and promotion of apoptosis of osteoblasts and osteocytes by glucocorticoids. Potential mechanisms of their deleterious effects on bone," *J. Clin. Invest.* **102**, 274–282 (1998).
- D. M. Reid, J.-P. Devogelaer, K. Saag, C. Roux, C.-S. Lau, J.-Y. Reginster, P. Papanastasiou, A. Ferreira, F. Hartl, T. Fashola, P. Mesenbrink, and P. N. Sambrook, "Zoledronic acid and risedronate in the prevention and treatment of glucocorticoid-induced osteoporosis (horizon): a multicentre, double-blind, double-dummy, randomised controlled trial," *Lancet* **373**, 1253–1263 (2009).
- S. Silverman, "New therapies for osteoporosis: zoledronic acid, bazedoxifene, and denosumab," *Cur. Osteoporosis Rep.* **7**, 91–95 (2009).
- J.-P. Devogelaer, R. A. Adler, C. Recknor, K. See, M. R. Warner, M. Wong, and K. Krohn, "Baseline glucocorticoid dose and bone mineral density response with teriparatide or alendronate therapy in patients with glucocorticoid-induced osteoporosis," *J. Rheumatol.* **37**, 141–148 (2010).
- B. Seriola, S. Paolino, A. Sulli, V. Ferretti, and M. Cutolo, "Bone metabolism changes during anti-TNF therapy in patients with active rheumatoid arthritis," *Ann. N.Y. Acad. Sci.* **1069**, 420–427 (2006).
- K. G. Saag, E. Shane, S. Boonen, F. Marin, D. W. Donley, K. A. Taylor, G. P. Dalsky, and R. Marcus, "Teriparatide or alendronate in glucocorticoid-induced osteoporosis," *N. Engl. J. of Med.* **357**, 2028–2039 (2007).
- K. G. Saag, J. R. Zanchetta, J.-P. Devogelaer, R. A. Adler, R. Eastell, K. See, J. H. Krege, K. Krohn, and M. R. Warner, "Effects of teriparatide versus alendronate for treating glucocorticoid-induced osteoporosis: thirty-six-month results of a randomized, double-blind, controlled trial," *Arthritis Rheum.* **60**, 3346–3355 (2009).
- D. Faibish, S. M. Ott, and A. L. Boskey, "Mineral changes in osteoporosis: a review," *Clin. Orthop. and Relat. Res.* **443**, 28–38 (2006).
- A. Carden and M. D. Morris, "Application of vibrational spectroscopy to the study of mineralized tissues (review)," *J. Biomed. Opt.* **5**, 259–268 (2000).
- B. R. McCreadie, M. D. Morris, T. Chen, D. S. Rao, W. F. Finney, E. Widjaja, and S. A. Goldstein, "Bone tissue compositional differences in women with and without osteoporotic fracture," *Bone (N.Y.)* **39**, 1190–1195 (2006).
- M. Raghavan, N. D. Sahar, R. H. Wilson, M.-A. Mycek, N. Pleshko, D. H. Kohn, and M. D. Morris, "Quantitative polarized Raman spectroscopy in highly turbid bone tissue," *J. Biomed. Opt.* **15**, 037001 (2010).
- K. A. Dehring, N. J. Crane, A. R. Smukler, J. B. McHugh, B. J. Roessler, and M. D. Morris, "Identifying chemical changes in subchondral bone taken from murine knee joints using Raman spectroscopy," *Appl. Spectrosc.* **60**, 1134–1141 (2006).
- J. Keffer, L. Probert, H. Cazarlis, S. Georgopoulos, E. Kaslaris, D. Kioussis, and G. Kollias, "Transgenic mice expressing human tumour necrosis factor: a predictive genetic model of arthritis," *EMBO J.* **10**, 4025–4031 (1991).
- P. Li and E. M. Schwarz, "The TNF- α transgenic mouse model of inflammatory arthritis," *Springer Semin. Immunopathol.* **25**, 19–33 (2003).
- N. E. Lane, W. Yao, M. Balooch, R. K. Nalla, G. Balooch, S. Habelitz, J. H. Kinney, and L. F. Bonewald, "Glucocorticoid-treated mice have localized changes in trabecular bone material properties and osteocyte lacunar size that are not observed in placebo-treated or estrogen-deficient mice," *J. Bone Miner. Res.* **21**, 466–476 (2006).
- F. W. Esmonde-White, K. A. Esmonde-White, and M. D. Morris, "Minor distortions with major consequences: correcting distortions in imaging spectrographs," *Appl. Spectrosc.* **65**, 85–98 (2011).
- K. A. Dooley, F. W. L. Esmonde-White, and M. D. Morris, "Optical fiber bundle coupling errors in Raman spectra: correction via data processing," *Proc. SPIE* **7560**, 75600O (2010).
- C. A. Lieber and A. Mahadevan-Jansen, "Automated method for subtraction of fluorescence from biological Raman spectra," *Appl. Spectrosc.* **57**, 1363–1367 (2003).
- A. Savitzky and M. J.E. Golay, "Smoothing and differentiation of data by simplified least squares procedures," *Anal. Chem.* **36**, 1627–1639 (1964).
- D. G. Reynolds, C. Hock, S. Shaikh, J. Jacobson, X. Zhang, P. T. Rubery, C. A. Beck, R. J. O'Keefe, A. L. Lerner, E. M. Schwarz, and H. A. Awad, "Micro-computed tomography prediction of biomechanical strength in murine structural bone grafts," *J. Biomech.* **40**, 3178–3186 (2007).
- J. J. Broz, S. J. Simske, A. R. Greenberg, and M. W. Luttgies, "Effects of rehydration state on the flexural properties of whole mouse long bones," *J. Biomech. Eng.* **115**, 447–449 (1993).
- M. D. Brodt, C. B. Ellis, and M. J. Silva, "Growing C57Bl/6 mice increase whole bone mechanical properties by increasing geometric and material properties," *J. Bone Miner. Res.* **14**, 2159–2166 (1999).
- M. J. Silva, M. D. Brodt, B. Wopenka, S. Thomopoulos, D. Williams, M. H. Wassen, M. Ko, N. Kusano, and R. A. Bank, "Decreased collagen organization and content are associated with reduced strength of demineralized and intact bone in the SAMP6 mouse," *J. Bone Miner. Res.* **21**, 78–88 (2006).
- D. M. Haaland and E. V. Thomas, "Partial least-squares methods for spectral analyses. I Relation to other quantitative calibration methods and the extraction of qualitative information," *Anal. Chem.* **60**, 1193–1202 (1988), <http://pubs.acs.org/doi/pdf/10.1021/ac00162a020>.
- D. Qi and A. J. Berger, "Chemical concentration measurement in blood serum and urine samples using liquid-core optical fiber Raman spectroscopy," *Appl. Opt.* **46**, 1726–1734 (2007).
- B. D. Beier, R. G. Q.Jr., and A. J. Berger, "Identification of different bacterial species in biofilms using confocal Raman microscopy," *J. Biomed. Opt.* **15**, 066001 (2010).
- P. Pennisi, A. Trombetti, and R. Rizzoli, "Glucocorticoid-induced osteoporosis and its treatment," *Clin. Orthop. Relat. Res.* **443**, 39–47 (2006).
- H. D. Nelson, M. Helfand, S. H. Woolf, and J. D. Allan, "Screening for postmenopausal osteoporosis: a review of the evidence for the U.S. preventive services task force," *Ann. Intern. Med.* **137**, 529–541 (2002), <http://www.annals.org/content/137/6/529.full.pdf+html>.
- M. V. Schulmerich, J. H. Cole, K. A. Dooley, M. D. Morris, J. M. Kreider, and S. A. Goldstein, "Optical clearing in transcutaneous Raman spectroscopy of murine cortical bone tissue," *J. Biomed. Opt.* **13**, 021108 (2008).
- M. V. Schulmerich, J. H. Cole, J. M. Kreider, F. Esmonde-White, K. A. Dooley, S. A. Goldstein, and M. D. Morris, "Transcutaneous Raman spectroscopy of murine bone *in vivo*," *Appl. Spectrosc.* **63**, 286–295 (2009).
- M. V. Schulmerich, K. A. Dooley, M. D. Morris, T. M. Vanasse, and S. A. Goldstein, "Transcutaneous fiber optic Raman spectroscopy of bone using annular illumination and a circular array of collection fibers," *J. Biomed. Opt.* **11**, 060502 (2006).
- M. V. Schulmerich, J. H. Cole, K. A. Dooley, M. D. Morris, J. M. Kreider, S. A. Goldstein, S. Srinivasan, and B. W. Pogue, "Noninvasive Raman tomographic imaging of canine bone tissue," *J. Biomed. Opt.* **13**, 020506 (2008).
- P. Matousek, E. R. C. Draper, A. E. Goodship, I. P. Clark, K. L. Ronayne, and A. W. Parker, "Noninvasive Raman spectroscopy of human tissue *in vivo*," *Appl. Spectrosc.* **60**, 758–763 (2006).
- O. Akkus, F. Adar, and M. B. Schaffler, "Age-related changes in physicochemical properties of mineral crystals are related to impaired mechanical function of cortical bone," *Bone* **34**, 443–453 (2004).
- J. S. Yerramshetty and O. Akkus, "The associations between mineral crystallinity and the mechanical properties of human cortical bone," *Bone* **42**, 476–482 (2008).
- X. Bi, C. A. Patil, C. C. Lynch, G. M. Pharr, A. Mahadevan-Jansen, and J. S. Nyman, "Raman and mechanical properties correlate at whole bone- and tissue-levels in a genetic mouse model," *J. Biomech.* **44**, 297–303 (2011).